Journal of the Serbian Chemical Society
JSCS-info@shd.org.rs • www.shd.org.rs/JSCS
J. Serb. Chem. Soc. *89* (5) 667–678 (2024)
JSCS–5747
Original scientific paper
Published 9 May 2024

The influence of the coprecipitation synthesis methods on photodegradation efficiency of ZnFe based photocatalysts

ĐURĐICA M. KARANOVIĆ[1]*, MILICA S. HADNAĐEV-KOSTIĆ[1], TATJANA J. VULIĆ[1], MARIJA M. MILANOVIĆ[1], VLADANA N. RAJAKOVIĆ-OGNJANOVIĆ[2] and RADMILA P. MARINKOVIĆ-NEDUČIN[1#]

[1]*Faculty of Technology Novi Sad, University of Novi Sad, Bulevar Cara Lazara 1, 21000 Novi Sad, Serbia and* [2]*Faculty of Civil Engineering, University of Belgrade, Bulevar Kralja Aleksandra 73, 11000 Beograd, Serbia*

(Received 6 November, revised 15 November 2023, accepted 22 January 2024)

Abstract: Organic dye pollutants that are progressively used in modern chemical industries, emerged as a major source of water contamination. A promising eco-friendly and simple approach to water purification is the heterogeneous photocatalytic process that uses various metal oxide semiconductors in the presence of light, initiating the oxidation-reduction reactions resulting in dye degradation. The aim of this study was to investigate the influence of coprecipitation synthesis methods on photodegradation efficiency. The ZnFe based photocatalysts were synthesized using two different methods: low (LS) supersaturation and high (HS) supersaturation coprecipitation and thermally activated at 100, 300, 500 and 700 °C. Structural and textural characterisation were carried out and their efficiency in methylene blue photodegradation test reaction was studied. LS samples treated at 100 and 300 °C exhibited very low photodegradation efficiency (less than 10 %) when compared to HS samples treated at the same temperatures (75 and 85 %). The efficiency of LS 500 and LS 700 samples improved (67 and 75 %) with the increase in thermal treatment temperature and the photodegradation efficiency difference between LS and HS samples decreased. Such behaviour of LS and HS samples could be explained by structural and textural properties that originated from different synthesis methods.

Keywords: mixed metal oxides; photocatalysis; methylene blue.

INTRODUCTION

Rapid industrial growth over past few decades had immense negative influence on water eco-systems due to the presence of organic and inorganic con-

* Corresponding author. E-mail: djurdjicakaranovic@uns.ac.rs
# Serbian Chemical Society member.
https://doi.org/10.2298/JSC231106005K

taminants such as synthetic dyes,[1,2] antibiotics,[3] pesticides,[4] *etc*. These micro--contaminants raised concerns due to their excessive use in various industries and their discharge to aquatic environment. Organic and inorganic dyes have the ability to persist in the water environment for a significant amount of time, because of their stability. Textile industry was reported to lose up to 200,000 tons of dyes to effluents due to inefficiency of the dyeing process.[5] Methylene blue (MB) is one of the organic dyes commonly used in industry and its presence in aquatic environment proved to be toxic.[6,7] Methods of purification of wastewater before its discharge in environment have been researched over the past few decades, and some of them include adsorption, membrane filtration, oxidation, bioremediation, ion-exchange and heterogenous photocatalysis.[8,9] The main disadvantage of many methods for water purification is the lack of capability to completely degrade hazardous pollutants.[10] Photocatalytic purification of wastewater using semiconductive oxides, such as TiO_2, ZnO and Fe_2O_3, received substantial attention since it could use free and sustainable solar energy, it is simple, rapid, environmentally friendly and leads to complete degradation of organic and inorganic contaminants.[11–14] The possible additional application of these photocatalytic materials could be in the infrastructure design introducing added-value to porous pavements for managing pluvial floods resulting in the reduction of water pollution.[15] Layered double hydroxides (LDHs) are described as anionic clays with layered structure, with metal cations uniformly distributed in the hydroxide layers. Their versatility brought about significant attention in the field of photocatalytic degradation of dyes. Upon thermal treatment of LDHs, their layered structure collapses, hydroxyls and interlayer water transition to gaseous phase, triggering the formation of mixed metal oxides.[16] The use of mixed metal oxides in photocatalytic purification of wastewater became very popular field of research, due to their reported ability to degrade various dyes,[17] pesticides,[18] antibiotics.[3] Mixed metal oxides are promising for the application in photocatalytic treatment of wastewater because of their favourable properties, such as strong oxidation ability, good photocatalytic properties and coupling with semiconductors.[19] For example, zinc oxide exhibited favourable photocatalytic properties, such as high stability, non-toxicity and, due to its large band gap of 3.37 eV, possible coupling with semiconductors with narrow energy band gap in order to ameliorate its photocatalytic performance.[20,21] ZnO could also be used as antibacterial agent, since it has been reported to have antibacterial influence on both Gram-positive and Gram-negative bacteria.[22] Furthermore, iron and its oxides are suitable for the photocatalytic application because of their stability, non-toxicity, magnetic and optical properties, abundance and low cost.[23] ZnFe mixed metal oxides obtained by thermal degradation of LDHs received much attention due to the possibility to tailor their functional properties during the synthesis

procedure resulting in the formation of nonstoichiometric mixed oxides with different additional phases, favourable for photocatalytic application.[16]

Various synthesis methods have been researched, including coprecipitation, sol–gel, hydrothermal, layer deposition and calcination of metal hydroxide precursor.[2,24,26] The coprecipitation synthesis method was selected taking into consideration that the synthesis path should be simple, cost-effective and environmentally friendly. The motivation behind this study was to apply a simple synthesis route that will enable the formation of photocatalysts with suitable properties for efficient photocatalytic application. Taking all of the above into account, the influence of synthesis method and thermal treatment on structural, textural and photocatalytic properties of obtained ZnFe photocatalysts was studied.

EXPERIMENTAL

Preparation of photocatalysts

Photocatalysts were synthesized using two synthesis methods: low supersaturation co-precipitation (LS) method at constant pH and high supersaturation (HS) coprecipitation method. For both synthesis methods the same base solution (0.67 M Na_2CO_3; 2.25 M NaOH) and metal precursors were used: $Fe(NO_3)_3 \cdot 9H_2O$ and $Zn(NO_3)_2 \cdot 6H_2O$ dissolved in 1 M solution containing 30 mol % of Fe and 70 mol % of Zn). In the LS method, the precursor solutions and the base solution were continuously added (4 cm^3 min^{-1}) at constant temperature (40 °C) maintaining the constant pH of 9.4 in the reaction mixture (Fig. 1a). In the HS method (Fig. 1b), the precursor solutions were quickly added to the base solution and vigorously stirred at constant temperature (40 °C). The precipitation products obtained from both synthesis methods were aged (12 h), washed with distilled water until pH 7, dried (24 h; 100 °C) and thermally treated at different temperatures (300, 500, 700 °C) for 5 h in air. The synthesized samples were denoted as follows: ZnFe LS 100, ZnFe LS 300, ZnFe LS 500, ZnFe LS 700, ZnFe HS 100, ZnFe HS 300, ZnFe HS 500, ZnFe HS 700.

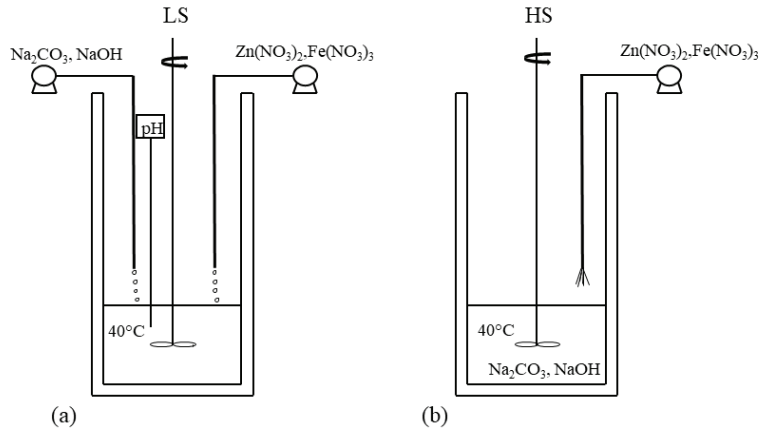

Fig. 1. Schemes of experimental set-ups for: a) LS and b) HS synthesis method.

Characterization of photocatalysts

X-ray powder diffraction (XRD) was used for the identification of crystalline phases. XRD analysis was conducted with Rigaku MiniFlex 600 with Cu-Kα radiation (λ = 0.15406 nm; 2θ range from 10 to 70°; scan rate = 0.02 s^{-1}). The crystallite size was calculated using the Scherrer formula:

$$D = k\frac{\lambda}{\beta\cos\theta} \tag{1}$$

where D, nm, is the crystallite size, k is the shape function (0.9), λ, nm, is X-ray wavelength, θ is angle of diffraction and β full width at half maximum of the most intense peak.

Textural analysis was performed by low temperature nitrogen adsorption at –196 °C (Microtrac Belsorp Max II). The surface area was calculated using the Brunauer–Emmer––Teller (BET) method. The pore size distribution and the cumulative pore volume were determined by Brunauer–Joyner–Hallenda (BJH) method applied to the desorption branch of the isotherm. The external surface area, which represented the mesopore surface area without micropores, was calculated using the *t*-plot method.

Photodegradation experiments

Photocatalytic tests were performed in an open cylindrical Pyrex vessel. Prior to the irradiation, all of the mixtures (100 ml of MB solution and 50 mg of photocatalyst) were stirred in the dark. The MB concentration was measured at defined time intervals using the UV–Vis spectrophotometer (Cecil2000) at maximum absorption length of 664 nm. The adsorption/desorption equilibrium was reached after 30 min. These tests were performed in order to ensure that photocatalytic efficiency of investigated samples was solely attributed to the photocatalytic reaction.

When the equilibrium was established, reaction mixtures were irradiated by the light source (Osram Ultra Vitalux 300 W lamp with the emission spectrum that simulates the solar light placed 45 cm above the top surface of MB solution) and aliquots were analysed at defined time intervals. The decrease in MB concentration was used to calculate the efficiency of MB photodegradation:[27,28]

$$E_{\text{eff}} = 100\frac{c_0 - c}{c} \tag{2}$$

E_{eff} , %, is the photodegradation efficiency, c_0, mg dm^{-3}, and c, mg dm^{-3}, are the initial and measured MB concentration.

Kinetics of the photocatalytic reaction

The kinetics of MB photodegradation reaction were evaluated using the pseudo-first--order reaction that follows the Langmuir–Hinshelwood kinetic model:[29]

$$\ln\left(\frac{c_0}{c_t}\right) = k_{\text{app}}t \tag{1}$$

The MB concentration at defined time t was denoted as c_t and k_{app} is the apparent first order reaction rate constant, obtained from the slope of linear function $\ln(c_0/c_t)$ *vs*. time.

The half-time of the reaction, $t_{1/2}$, was calculated as follows:

$$t_{1/2} = \frac{\ln 2}{k_{\text{app}}} \tag{4}$$

RESULTS AND DISCUSSION

Structural characterization

XRD diffraction peaks of all synthesized and thermally treated photocatalysts, presented in Fig. 2, can be correlated with the series of Bragg reflections corresponding to the standard JCPDS. XRD patterns of ZnFe LS 100 in Fig. 2a exhibited low intensity broad peaks characteristic for the layered structure (2θ values of 13.18, 23.97, 32.72 and 59.27°) which correspond to (003), (006), (009) and (110) planes,[30] with additional low intensity broad peaks (32.6 and 36.2°) that could be attributed to the ZnO phase. XRD analysis of the dried sample obtained by the HS method (ZnFe HS 100) revealed the presence of sharp, intense peaks of dominant (31.8, 34.4, 47.5, 56.6, 62.8°) zincite ZnO phase. Considering that the dominant phase of LS sample was typical for the layered structure, it can be concluded that the LS synthesis method triggered the formation of ZnFe layered double hydroxide, whereas the HS method led to formation of non-stoichiometric mixed metal oxides.

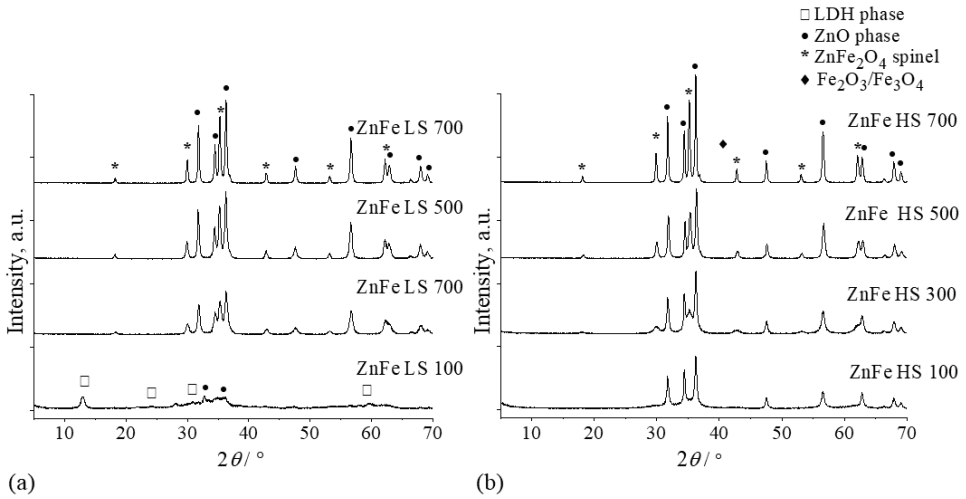

Fig. 2. XRD pattern of photocatalysts: a) LS samples and b) HS samples.

After thermal treatment of LS samples at temperatures above 300 °C (ZnFe LS 300), the layered structure collapsed and intense, sharp peaks were detected corresponding to the zincite ZnO phase (JCPDS File no. 79-2205). Additionally, new, lower intensity peaks (30, 35.4, 42.8 and 52.9°) were detected in both LS and HS samples treated at 300 °C that confirmed the formation of $ZnFe_2O_4$ spinel phase (JCPDS file no. 89-1012). For samples obtained by both LS and HS method the increase in thermal treatment temperature (500 and 700 °C) intensified the crystallisation of the phases detected by the presence of sharp, more

intense and distinctive peaks of both, dominant zincite ZnO phase and additional $ZnFe_2O_4$ spinel phase. Additionally, in both LS and HS samples thermally treated at 700 °C the appearance of low-intensity peak was detected at 2θ value of around 37° that could be correlated to the Fe_2O_3 or Fe_3O_4 phase (JCPDS file no. 87-2334).[31,32] The crystallite size calculated for the dominant phase (Table I), also confirmed the increase of crystallite size with the rise of thermal treatment temperature, considering that the temperature increase generally results in the grain growth and consequently in greater crystallite size.[16,31,32] When compared with the HS samples, LS samples exhibited similar crystal structure at higher temperatures with lower peak intensities, indicating lower crystallinity of LS samples. The XRD analysis results showed significant influence of synthesis method on the crystal structure of studied samples.

TABLE I. Structural and textural parameters of analysed samples

Sample	D / nm	S / m^2 g^{-1}	d_p / nm	V_p / cm^3 g^{-1}	S_{tp} / m^2 g^{-1}
ZnFe LS 100	9.6	82	14.9	0.36	80.8
ZnFe LS 300	15.8	28.5	46.9	0.32	28
ZnFe LS 500	22.6	27	40.5	0.26	25.4
ZnFe LS 700	28.1	12.6	80.7	0.22	12.6
ZnFe HS 100	20.7	147	4.8	0.16	145.1
ZnFe HS 300	22.4	108	5.1	0.17	107.4
ZnFe HS 500	25.5	16.3	22.7	0.11	16
ZnFe HS 700	33.7	7.8	39.22	0.08	7.5

Textural charaterization

The results of textural analysis are given in Fig. 3 and Table I. The adsorption isotherms and pore size distribution of all studied samples are presented in Fig. 3. BET surface area, S, average pore diameter, d_p, pore volume, V_p, and external surface area obtained from t-plot method, S_{tp}, are given in Table I. The isotherms of LS samples (Fig. 3a) corresponded to type II isotherm from IUPAC classification. This type of isotherm is characteristic for non-porous or macroporous adsorbents and it represented unrestricted monolayer/multilayer adsorption. Type IV isotherms correspond to HS samples (Fig. 3b) and are characterized by the finite multi-layer formation that corresponds to complete filling of capillaries in an adsorbent. The mesoporous isotherms should be classified in more details if the hysteresis loop (where adsorption and desorption curves do not overlay) is present. LS samples exhibited H3 hysteresis loop type, indicating that LS samples had mesoporous structure with wedge shaped pores formed by the loose stacking of flaky particles.[33] Whereas for HS samples, hysteresis loops correspond to combination of H1/H3 types formed at relative pressure range of 0.4–1, concluding that present mesopores have non uniform shape.[31]

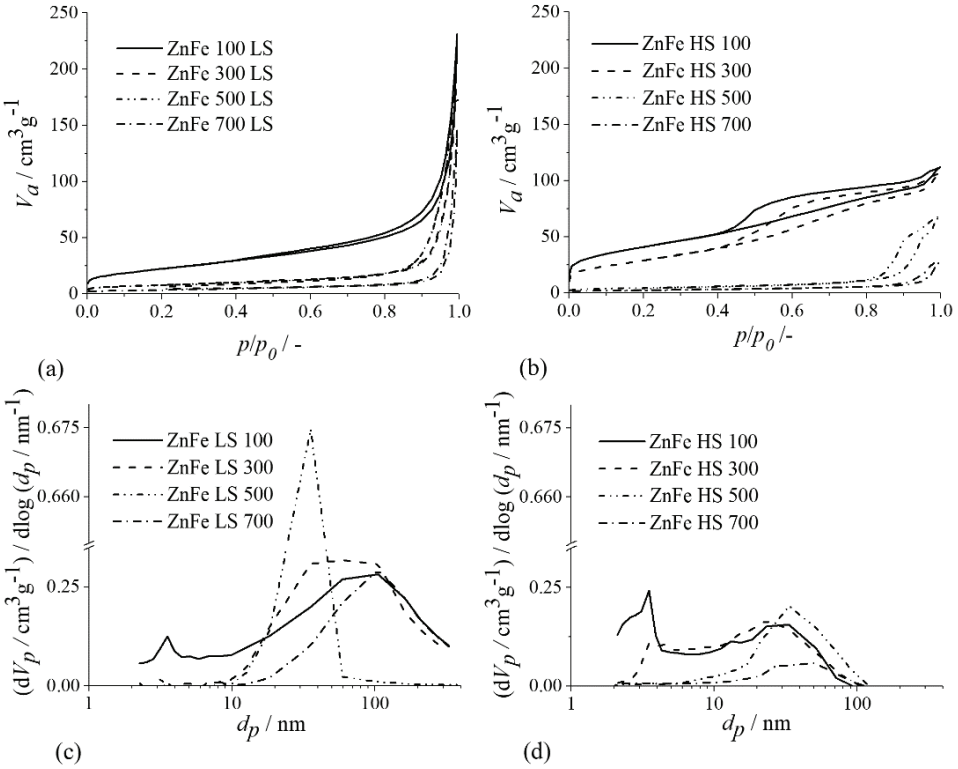

Fig. 3. Textural analysis results: a) adsorption isotherms for LS samples; b) adsorption isotherms for HS samples; c) pore size distribution for LS samples; d) pore size distribution for HS samples.

From Fig. 3c it was observed that the ZnFe LS 100 sample had a developed pore size distribution with an intense peak at around 3 nm that is in good agreement with the detected high surface area (Table I) and a wide peak at higher values of pore diameters (40–110 nm). ZnFe LS 300 sample exhibited a broad peak in the region of pore diameters from 30 to 100 nm. Upon the thermal treatment at 500 °C, sample ZnFe LS 500 showed monomodal pore size distribution with one intense peak at around 35 nm, whereas the sharp peak at 3 nm completely disappeared, which is in correlation with smaller measured pore volume.[31] The pore size distribution of sample ZnFe LS 700 shifted towards higher pore diameter values (> 50 nm), also in correlation to the significantly low surface area (Table I).

The pore size distribution of HS samples (Fig. 3d) was similar to LS samples, with a larger amount of smaller mesopores resulting in the much larger surface area. With the increase in the temperature of the HS sample thermal treatment, the presence of both, smaller and larger mesopores decreased, especially

for the samples treated at 500 and 700 °C BET surface area of LS samples treated at lower temperatures (100 and 300 °C), when compared to the corresponding HS samples, was significantly lower since it originated from the presence of mainly larger pores in those samples.[13] Pore size distribution and its change with temperature indicated that the increase in thermal treatment temperature shifted the pore size distribution towards higher values of pore diameters, which is in good correlation with measured parameters (a decrease in pore volume and BET surface area and an increase in average pore diameter).

The results obtained from textural analysis were also analysed by *t*-plot method.[34] The calculated external surface area is in good agreement with the calculated BET surface area, since it represented the surface area only from mesopores. These results confirmed that there were no micropores present in any of the samples.

Photodegradation of methylene blue

The results of the MB photodegradation (Fig. 4) showed that all the HS samples have significant photodegradation efficiency higher than the corresponding LS samples. Besides that, the LS samples treated at lower temperatures (100 and 300 °C) had very low efficiency (< 10 %). The results also indicate that the increase in thermal treatment temperature increased the photodegradation efficiency for samples obtained by both coprecipitation methods. Photocatalytic behaviour could be explained by the presence of photocatalytic active phases. All HS samples have photocatalytic active ZnO phase, whereas the samples treated at higher temperatures (ZnFe HS 300, ZnFe HS 500 and ZnFe HS 700) also have an additional $ZnFe_2O_4$ phase. The coupling of ZnO and $ZnFe_2O_4$ phases with energy bands from 2.1 to 2.3 eV, enhanced the MB photodegradation in the solar light spectrum.[31] Lower photodegradation efficiency of LS samples could be

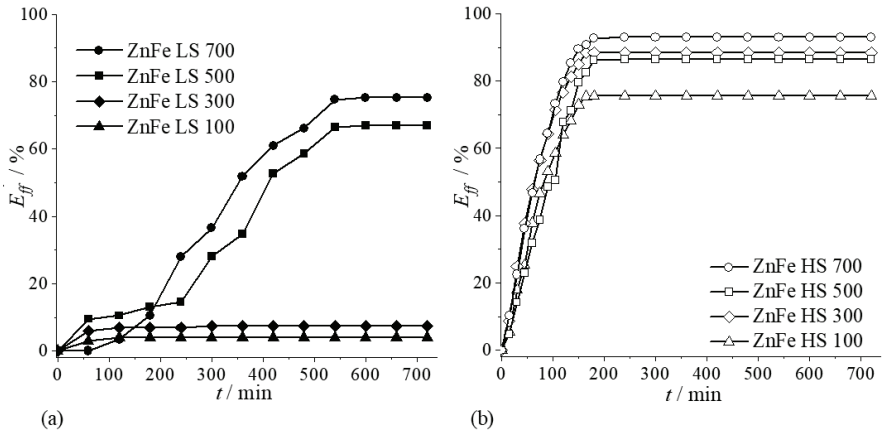

Fig. 4. Photodegradation efficiency of: a) LS photocatalysts and b) HS photocatalysts.

attributed to the lower presence and lower crystallinity of active phases, when compared to the corresponding HS samples, especially for the ZnFe LS 100 sample being the only sample with the LDH phase and the lowest amount of ZnO phase. Higher photodegradation efficiency (67 and 75 %) was observed for LS samples thermally treated at 500 and 700 °C probably due to the higher amount of $ZnFe_2O_4$ spinel phase. The enhanced photodegradation efficiency of ZnFe HS 700 (96 %), when compared to the corresponding LS sample, could be assigned to the higher amount of photocatalytic active ZnO, $ZnFe_2O_4$ phase and Fe_2O_3 phase which could allow easier transport of photo-induced electrons from $ZnFe_2O_4$.[14] It could be concluded that the favourable textural properties without the presence of adequate active phases did not have great impact on the photocatalytic behaviour.

Kinetics of photocatalytic reaction

The results of the kinetic study indicated that the experimental data obtained from MB photodegradation experiments were best fitted with the linear fit and followed the pseudo-first-order reaction model. The correlation coefficient was proposed as the best criteria for selection of kinetic model. The calculated values of the rate constant (Table II), as well as the half time of the reaction, for HS samples treated at 500 and 700 were approximately 5 times higher than rate constant values for LS samples treated at same temperatures, which confirmed that ZnFe HS 500 and 700 samples participated in faster reactions. The obtained results from the kinetic study showed that MB photodegradation followed Langmuir–Hinshelwood kinetic model, since photodegradation reactions with single substrate usually follow this model.[35]

TABLE II. Kinetic parameters of analysed samples

Sample	k_{app} / min^{-1}	$t_{1/2}$ / min	R^2	Sample	k_{app} / min^{-1}	$t_{1/2}$ / min	R^2
ZnFe LS 100	–	–	–	ZnFe HS 100	0.0084	82.5	1
ZnFe LS 300	-	–	–	ZnFe HS 300	0.0120	57.8	1
ZnFe LS 500	0.0022	315.1	0.96	ZnFe HS 500	0.0094	73.7	0.97
ZnFe LS 700	0.0017	407.7	0.95	ZnFe HS 700	0.0136	51.0	1

Since Langmuir–Hinshelwood kinetic model can be used under the following assumptions: *i*) limited amount of adsorption sites on photocatalyst surface, *ii*) monolayer coverage, *iii*) reversible adsorption reaction and *iv*) homogenous surface of photocatalysts; it could be concluded that the nature of active sites and their distribution had great influence on the rate of photocatalytic reaction and the rate of the entire process depended on the reaction carried out on the surface active sites.[29]

CONCLUSION

The mixed metal oxides obtained by low and high supersaturation co-precipitation methods were analysed and their efficiency was evaluated in MB photodegradation reaction. Both HS and LS samples exhibited desirable photocatalytic properties when thermally treated at higher temperatures due to the favourable structural and textural properties. It could be concluded that the photocatalytic active phases and the high crystallinity detected by XRD were responsible for good photocatalytic behaviour of HS samples. Furthermore, it could be concluded that the favourable textural properties without the presence of the adequate active phases did not have great impact on the photocatalytic behaviour. The study revealed that the HS sample treated at 700 °C had the highest efficiency in MB removal, probably due to the largest amount of active phases (ZnO, $ZnFe_2O_4$ and Fe_2O_3/Fe_3O_4). The reaction kinetics corresponded to the Langmuir–Hinshelwood pseudo-first order model. This study demonstrated that the synthesis path had a significant influence on the photocatalytic active phase formation and consequently on the MB photodegradation efficiency.

Acknowledgement. This research was supported by the Science Fund of the Republic of Serbia, Grant No. 7737365, Zero-Waste Concept for Flood Resilient Cities – Ø-Waste-Water and by the Ministry of Science, Technological Development and Innovation of the Republic of Serbia (Grant No. 451-03-47/2023-01/ 200134).

ИЗВОД

УТИЦАЈ КОПРЕЦИПИТАЦИОНЕ МЕТОДЕ СИНТЕЗЕ НА ЕФИКАСНОСТ ФОТОКАТАЛИЗАТОРА НА БАЗИ ZnFe

ЂУРЂИЦА М. КАРАНОВИЋ[1*], МИЛИЦА С. ХАДНАЂЕВ-КОСТИЋ[1], ТАТЈАНА Ј. ВУЛИЋ[1], МАРИЈА М. МИЛАНОВИЋ[1], ВЛАДАНА Н. РАЈАКОВИЋ-ОГЊАНОВИЋ[2] и РАДМИЛА П. МАРИНКОВИЋ-НЕДУЧИН[3]

[1]Технолошки факултет Нови Сад, Универзитет у Новом Саду, булевар цара Лазара 1 , 21000 Нови Сад, [2]Грађевински факултет, Универзитет у Београду, Булевар Краља Александра 73, Београд и [3]Универзитет у Новом Саду, Др Зорана Ђинђића 1, 21000 Нови Сад

Органски полутанти, попут боја, су веома заступљени у савременој хемијској индустрији, због чега су постали велик извор загађења. Хетерогена фотокатализа представља једноставан и еколошки повољан процес пречишћавања отпадних вода. Као фотокатализатори користе се различити полупроводници у виду металних оксида који у присуству светлости разграђују полутанте низом оксидо-редукционих реакција. Циљ овог истраживања је испитивање утицаја копреципитационе методе на ефикасност фоторазградње. Фотокатализатори на бази ZnFe су синтетисани користећи две копреципитационе методе: методу малог (LS) и великог (HS) презасићења и термички активирани на температурама од 100, 300, 500 and 700 °C. Анализиране су њихове структурне и тесктуралне особине, као и ефикасност фотокаталитичке разградње метиленског плавог. LS узорци термички третирани на 100 и 300 °C су показали веома малу ефикасност разградње боје (< 10 %) у поређењу са HS узроцима третираним на истим температурама (75 и 85 %). Са порастом температуре термичке активације повећала се ефикасност LS 500 и LS 700 узорка (67 и 75 %), а разлика у ефикасности LS и HS узорака се смањила.

Овакво понашање LS и HS узорака се може објаснити разликама у текстуралним и структурним особинама које потичу од различитих метода синтезе.

(Примљено 6. новембра, ревидирано 15. новембра 2023, прихваћено 22. јануара 2024)

REFERENCES

1. L. Mohapatra, K. M. Parida, *Sep. Purif. Technol*. **91** (2012) 73 (https://doi.org/10.1016/j.seppur.2011.10.028)
2. Z. Meng, M. Wu, Y. Yu, F. Meng, A. Liu, S. Komarneni, Q. Zhang, *Appl. Clay Sci*. **161** (2018) 1 (https://doi.org/10.1016/j.clay.2018.04.008)
3. R. Langbehn, C. Michels, H. Moreira Soares, *Environ. Pollut.* **275** (2021) 116603 (https://doi.org/10.1016/j.envpol.2021.116603)
4. I. A. Saleh, N. Zouari, M. A. Al-Ghouti, *Environ. Technol. Innov*. **19** (2020) 101026 (https://doi.org/10.1016/j.eti.2020.101026)
5. C. J. Ogugbue, T. Sawidis, *Biotechnol. Res. Int.* **2011** (2011) 967925 (https://doi.org/10.4061/2011/967925)
6. C. Srinivas, C. Nagamani, M. Gangadhar, M. Raja Sekhar, *Asian J. Chem.* **22** (2010) 5045 (https://asianjournalofchemistry.co.in/user/journal/viewarticle.aspx?ArticleID=22_7_11)
7. S. Pandey, J. Y. Do, J. Kim, M. Kang, *Int. J. Biol. Macromol*. **143** (2020) 60 (https://doi.org/10.1016/j.ijbiomac.2019.12.002)
8. M. Hadnadjev-Kostic, T. Vulic, Dj. Karanovic, M. Milanovic, *J. Serb. Chem. Soc*. **87** (2022) 1011 (https://doi.org/10.2298/JSC220228034H)
9. B. G. Ankamwar, V. B. Kamble, J. I. Annsi, L. S. Sarma, C. M. Mahajan, *J. Nanosci. Nanotechnol.* **17** (2017) 1185 (https://doi.org/10.1166/jnn.2017.12579)
10. G. Zhao, L. Liu, C. Li, T. Zhang, T. Yan, J. Yu, X. Jiang, F. Jiao, *J. Photochem. Photobiol., A* **367** (2018) 302 (https://doi.org/10.1016/j.jphotochem.2018.08.048)
11. K. Abderrazek, F.S. Najoua, E. Srasra, *Appl. Clay Sci.* **119** (2016) 229 (https://doi.org/10.1016/j.clay.2015.10.014)
12. I. Ahmad, S.B. Khan, T. Kamal, A.M. Asiri, *J. Mol. Liq* **229** (2017) 429 (https://doi.org/10.1016/j.molliq.2016.12.061)
13. M. Hadnadjev-Kostic, T. Vulic, R. Marinkovic-Neducin, D. Lončarević, J. Dostanić, S. Markov, D. Jovanović, *J. Clean Prod.* **164** (2017) 1 (https://doi.org/10.1016/j.jclepro.2017.06.091)
14. S. Sun, X. Yang, Y. Zhang, F. Zhang, J. Ding, J. Bao, C. Gao, *Prog. Nat. Sci. Mater.* **22** (2012) 639 (http://dx.doi.org/10.1016/j.pnsc.2012.11.008)
15. O. Govedarica, M. Aškrabic, M. Hadnadev-Kostic, T. Vulic, B. Lekic, V. Rajakovic-Ognjanovic, D. Zakic, *Materials* **15** (2022) 4919 (https://doi.org/10.3390/ma15144919)
16. B. Kim, D. Lee, G. Gwak, Y. Han, J. Oh, *J. Solid State Chem.* **269** (2019) 454 (https://doi.org/10.1016/j.jssc.2018.10.013)
17. M. Sánchez-Cantú, M.E. Hernández-Torres, A. Castillo-Navarro, E. Cadena-Torres, E. Rubio-Rosas, E., Gracia-Jiménez, J.M., Tzompantzi, F., *Appl. Clay Sci.* **135** (2017) 1 (https://doi.org/10.1016/j.clay.2016.08.028)
18. E.S. da Silva, V. Prevot, C. Forano, P. Wong-Wah-Chung, H.D. Burrows, M. Sarakha, *Environ. Sci. Pollut. Res*. **21** (2014) 11218 (https://doi.org/10.1007/s11356-014-2971-z)
19. S. B. Jaffri, K. S. Ahmad, *Green Process Synth.* **8** (2019) 172 (https://doi.org/10.1515/gps-2018-0058)

20. J. Gajendiran, V. Rajendran, *Mater. Lett*. **116** (2014) 311 (https://doi.org/10.1016/j.matlet.2013.11.063)
21. C. Han, M.Q. Yang, B. Weng, Y. Xu, *Phys. Chem. Chem. Phys.* **16** (2014) 16891 (https://doi.org/10.1039/c4cp02189d)
22. A. E. A. Yagoub, G. M. Al-Shammari, L. N. Al-Harbi, P. Subash-Babu, R. Elsayim, M. A. Mohammed, M. A. Yahya, *Appl. Sci.* **12** (2022) 11613 (https://doi.org/10.3390/app122211613)
23. M. Afkari, S. M. Masoudpanah, M. Hasheminiasari, S. Alamolhoda, *Sci. Rep.* **13** (2023) 6203 (https://doi.org/10.1038/s41598-023-33338-1)
24. M. T. Uddin, Y. Nicolas, C. Olivier, T. Toupance, L. Servant, M. M. Müller, H. J. Kleebe, J. Ziegler, W. Jaegermann, *Inorg. Chem.* **51** (2012) 7764 (https://doi.org/10.1021/ic300794j)
25. A. M. Tripathi, R. G. Nair, S. K. Samdarshi, *Sol. Energy Mater. Sol. Cells* **94** (2010) 2379 (https://doi.org/10.1016/j.solmat.2010.08.022)
26. Y. Shen, T. R. B. Foong, X. Hu, *Appl. Catal., A* **409**–**410** (2011) 87 (https://doi.org/10.1016/j.apcata.2011.09.033)
27. S. Kurajica, I. Minga, R. Blazic, K. Muzina, P. Tominac, *Athens J. Sci.* **5** (2018) 7 (https://doi.org/10.30958/ajs.5-1-1)
28. I. Raheb, M. S. Manlla, *Heliyon* **7** (2021) (https://doi.org/10.1016/j.heliyon.2021.e07427)
29. M. Hadnadjev-Kostic, T. Vulic, R. Marinkovic-Neducin, *Adv. Powder Technol*. **25** (2014) 1624 (https://doi.org/10.1016/j.apt.2014.05.015)
30. D. Moustafa, R. Mahmoud, H. M. A. El Salam, N. Shehata, *Appl. Nanosci*. **11** (2021) 709 (https://doi.org/10.1007/s13204-020-01632-3)
31. M. Hadnadjev-Kostic, Dj. Karanovic, T. Vulic, J. Dostanić, D. Lončarević, *Green Process. Synth.* **12** (2023) 20228153 (https://doi.org/10.1515/gps-2022-8153)
32. X. Liu, F. Zhu, W. Wang, J. Lei, G. Yin, *Int. J. Electrochem. Sci.* **11** (2016) 9696 (https://doi.org/10.20964/2016.11.62)
33. Z. Wang, X. Jiang, M. Pan, Y. Shi, *Minerals* **10** (2020) 377 (https://doi.org/10.3390/min10040377)
34. A. Galarneau, F. Villemot, J. Rodriguez, F. Fajula, B. Coasne*, Langmuir* **30** (2014) 13266 (https://doi.org/10.1021/la5026679)
35. L. el Mersly, E. M. el Mouchtari, E. M. Moujahid, C. Forano, M. el Haddad, S. Briche, A. Alaoui Tahiri, S. Rafqah, *J. Sci-Adv. Mater. Dev*. **6** (2021) 118 (https://doi.org/10.1016/j.jsamd.2020.08.002).